Supporting Information for

Semiconducting Edges and Flake-Shape Evolution of Monolayer GaSe: Role of Edge Reconstructions

Ning Wang,[a,b] Dan Cao,[a,] Jun Wang,[b] Pei Liang,[b] Xiaoshuang Chen,[c] and Haibo Shu, [b,c,*]*

[a]College of Science and [b]College of Optical and Electronic Technology, China Jiliang University, 310018 Hangzhou, China

[c]National Laboratory for Infrared Physics, Shanghai Institute of Technical Physics, Chinese Academy of Science, 200083 Shanghai, China

Corresponding author

*E-mail address: caodan@cjlu.edu.cn, shu123hb@gmail.com

S1. Atomic configurations of zigzag and armchair GaSe edges

GaSe (or InSe) edges are investigated by using the nanoribbon models. The GaSe (or InSe) nanoribbons are created by cutting the ribbons from a perfect GaSe (or InSe) nanosheet with desired width and edges. There are two basic edge types: armchair (AC) and zigzag (ZZ) edges. Owing to the lack of in-plane inversion symmetry, the ZZ edges have two types: Metal-terminated (ZZ-M) and Se-terminated (ZZ-Se) edges. In this work, we investigate fourteen edge structures by considering different edge reconstructions and configurations, including five ZZ-M (M = Ga, In) edges (see Fig. S1a–e), six ZZ-Se edges (Fig. S1f–k), and three AC edges (Fig. S2). In Fig. S1, R1, R2, and R3 denote the (1×1), (2×1), and (3×1) edge reconstructions, respectively.

As shown in Fig. S1a and b, M-R1-1 and M-R1-2 are the (1×1) reconstructed ZZ-M edge with Ga-termination and Se-dimer termination, respectively. M-R2-1 is a (2×1) reconstructed ZZ-M edge (Fig. S1c), and M-R3-1 (Fig. S1d) and M-R3-2 (Fig. S1e) are the (3×1) reconstructed ZZ-M edge with two alternative Se atoms and an M vacant, respectively. Se-R1-1 (Fig. S1f) and Se-R1-2 (Fig. S1g) are (1×1) reconstructed ZZ-Se edge with Se-termination and Ga-dimer termination, respectively. Se-R2-1 (Fig. S1h) is a (2×1) reconstructed ZZ-Se edge, and Se-R3-1 (Fig. S1i), Se-R3-2 (Fig. S1j), and Se-R3-3 (Fig. S1k) are the (3×1) reconstructed ZZ-M edge with an opened termination, two M atoms, and a Se vacant, respectively. AC-P, AC-M, and AC-Se edges are the AC edge with the M-Se dimer termination, M-dimer termination, Se-dimer termination (Fig. S2a-c), respectively.

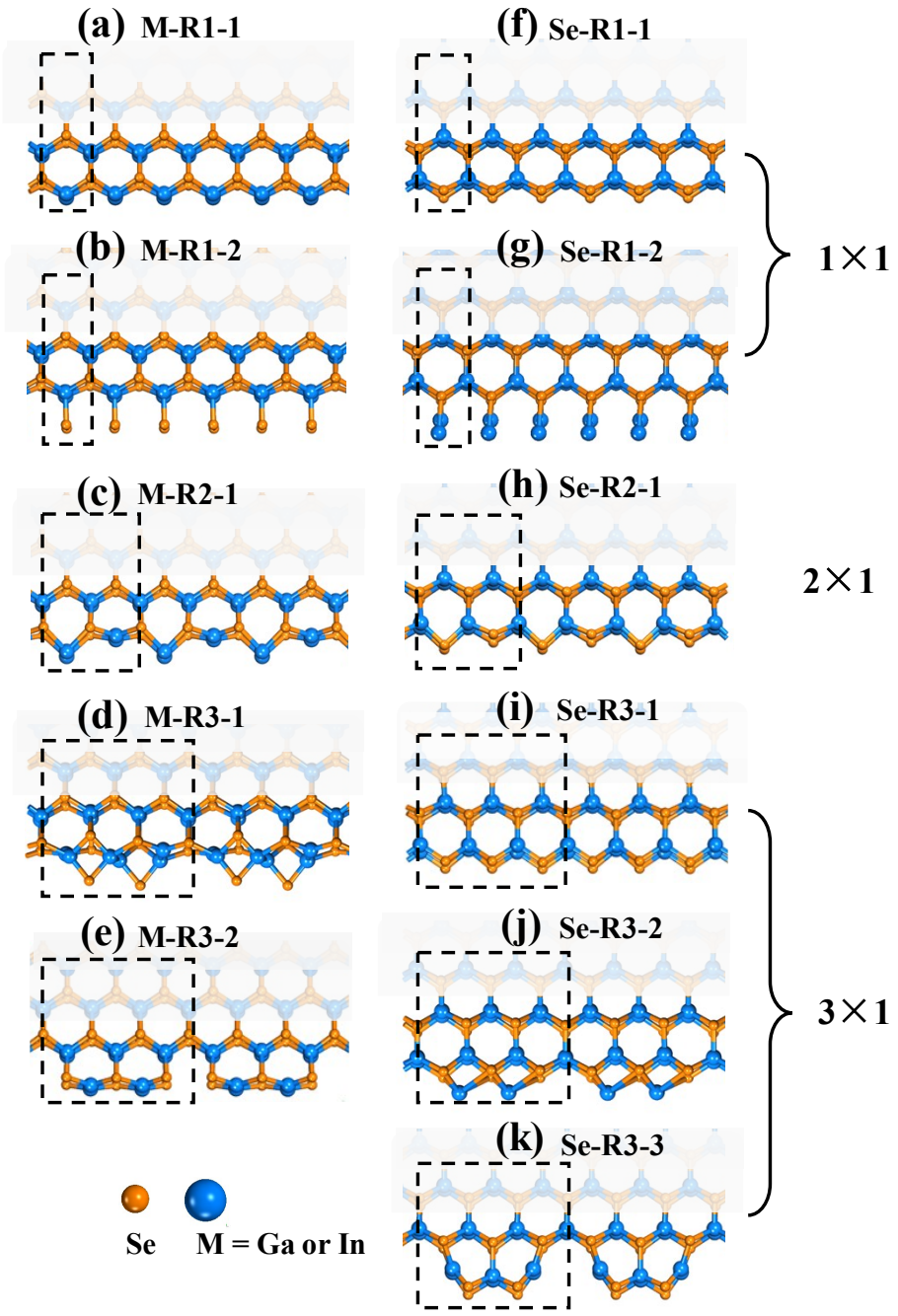

Fig. S1 Optimized atomic configurations of zigzag MSe (M = Ga, In) edges. (a) Perfect flat ZZ-M edge (M-R1-1), (b) Se-terminated ZZ-M edge (M-R1-2), (c) (2×1) reconstructed ZZ-M edge (M-R2-1), (d) (3×1) reconstructed ZZ-M edge terminated by two alternative Se atoms (M-R3-1), (e) (3×1) reconstructed ZZ-M edge with a M vacant (M-R3-2), (f) perfect flat ZZ-Se edge (Se-R1-1), (g) M-terminated ZZ-Se edge (Se-R1-2), (h) (2×1) reconstructed ZZ-Se edge (Se-R2-1), (i) (3×1) reconstructed ZZ-Se edge with a opened termination (Se-R3-1), (j) (3×1) reconstructed ZZ-Se edge terminated by two M atoms (Se-R3-2), and (k) (3×1) reconstructed ZZ-Se edge with a Se vacant (Se-R3-3). Blue and orange balls represent M and Se atoms, respectively.

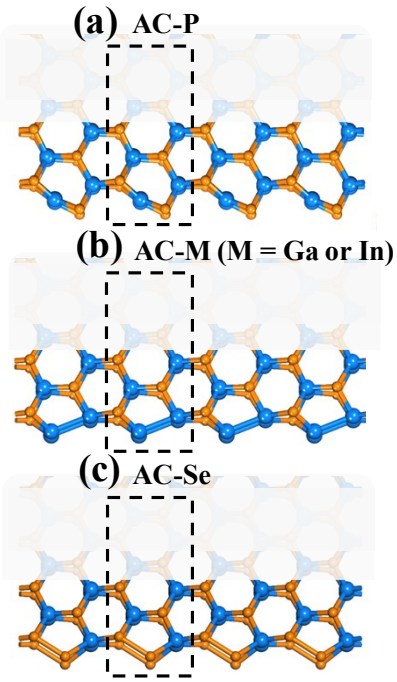

Fig. S2 Optimized atomic configurations of armchair MSe (M = Ga, In) edges. (a) Perfect flat AC edge (AC-P), (b) M-terminated AC edge (AC-M), and (c) Se-terminated AC edge (AC-Se). Blue and orange balls represent M and Se atoms, respectively.

S2. Computational details of edge formation energies

To facilitate our description, we use GaSe as an example to show the calculated detail about the edge formation energies of monolayer MX systems. The formation energy of an armchair (AC) edge (γ_A) is directly calculated by using an armchair nanoribbon model as follows,

$$\gamma_{\mathrm{A}} = (E_A - n\mu_{GaSe}) / 2L_A \tag{1}$$

where E_A is the total energy of an AC nanoribbon, n is the number of GaSe unit in the ribbon, μ_{GaSe} is the energy of GaSe unit in the monolayer sheet, and L_A is the length of AC ribbon along its periodic direction. Unlike the AC edges, formation energies (γ_Z) of zigzag (ZZ) edges cannot be directly calculated by the nanoribbon models due to the lack of inversion planar symmetry. To solve this problem, the triangular model with same zigzag edges (see Fig. S3) is used. The formation energy of a triangular GaSe flake with the side length l can be estimated by

$$\gamma = E_Z - n_{\mathrm{Ga}}\mu_{Ga} - n_{Se}\mu_{Se} = 3l\gamma_Z + 3\gamma_V \tag{2}$$

where E_Z is the total energy of triangular GaSe, n_{Ga} and n_{Se} are the number of Ga and Se atoms in the structure, γ_Z and γ_V are the formation energy of a ZZ edge and the vertex in the triangle model respectively. μ_{Ga} and μ_{Se} are the chemical potential of Ga and Se species, respectively. To maintain the thermodynamic equilibrium ($\mu_{GaSe} = \mu_{Ga} + \mu_{Se}$) of GaSe edges, the allowable value of μ_{Se} is $\mu_{\mathrm{Se(bulk)}}$-ΔH_f < μ_{Se} <$\mu_{\mathrm{Se(bulk)}}$, where the upper (lower) limit corresponds to Se-rich (Ga-rich) condition and ΔH_f is the heat of formation (1.23 eV). It seen from eq. (2) that γ_{Z} is transformed into a problem of eliminating the effect of vertexes, which can be realized by taking the energy difference between two similar triangle models with different side lengths. As shown in Fig. S3, by shrinking the length from l_1 to l_2, one has

$$\begin{cases} \gamma_Z = (\Delta E_Z - \Delta n_{Ga}\mu_{GaSe} - \Delta n\mu_{Se}) / 3(l_1 - l_2), \\ \Delta n_{Ga} = n_{Ga}(l_1) - n_{Ga}(l_2), \\ \Delta n = n_{Se}(l_1) - n_{Se}(l_2) - 2(n_{Ga}(l_1) - n_{Ga}(l_2)) \end{cases} \tag{3}$$

where ΔE_Z is the difference of total energy between triangular GaSe models with the

side lengths of l_1 and l_2. For an arbitrary chiral edge with a chiral angle χ, it contains both ZZ and AC sites. Therefore, the formation energy $\gamma(\chi)$ of a chiral edge can be described by[1-3]

$$\gamma(\chi) = |\gamma| \cos(\chi + C) \tag{4}$$

Where the direction of AC edge is set to χ =0, $|\gamma| = 2(\gamma_A^2 + \gamma_{Zx}^2 - \sqrt{3}\gamma_A\gamma_{Zx})^{1/2}$ and $C = \mathrm{sgn}(\chi) \cdot \arctan(\sqrt{3} - 2\gamma_{Zx}/\gamma_A)$ with the subscript x = Se at -30° <χ<0 or x=Ga at 0<χ<30°. Based on this equation, formation energy of arbitrary edge can be obtained as the basic energies γ_A and γ_{Zx} are known.

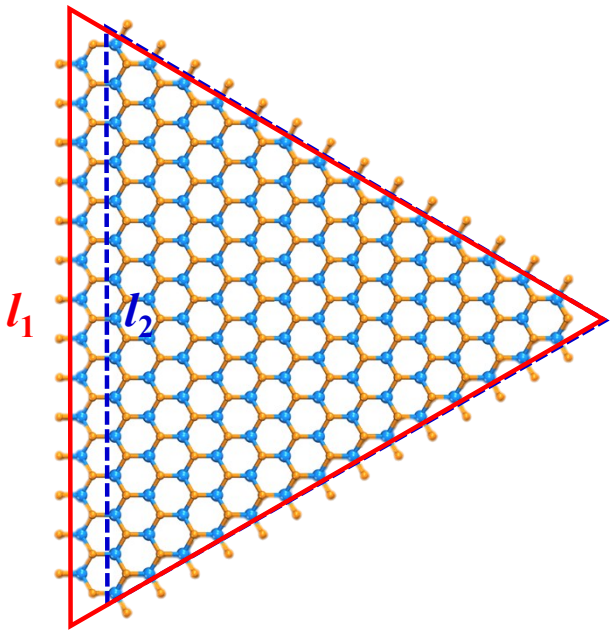

Fig. S3 Optimized atomic configurations of armchair MSe (M = Ga, In) edges. (a) perfect flat AC edge (AC-P), (b) M-terminated AC edge (AC-M), and (c) Se-terminated AC edge (AC-Se). Blue and orange balls represent M and Se atoms, respectively.

S3. Size-dependent formation energies of GaSe edges

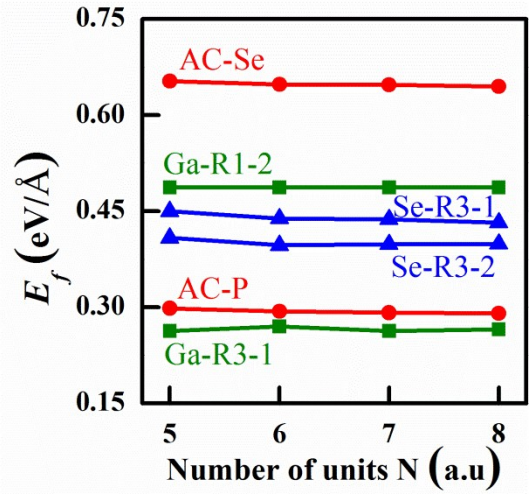

Fig. S4 Formation energies (E_f) of various GaSe edges with Ga-rich condition as a function of the size (N) of unit cell (or ribbon width).

S4. Formation energies of InSe edges

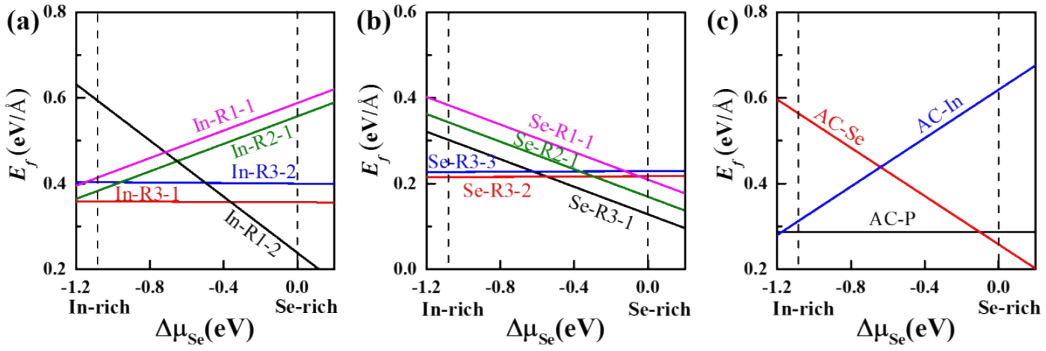

Fig. S5 Formation energies of (a) ZZ-In edges, (b) ZZ-Se edges, and (c) AC edges in InSe as a function of Se chemical potential difference ($\Delta\mu_{Se}$).

S5. Stability of zigzag GaSe nanoribbons

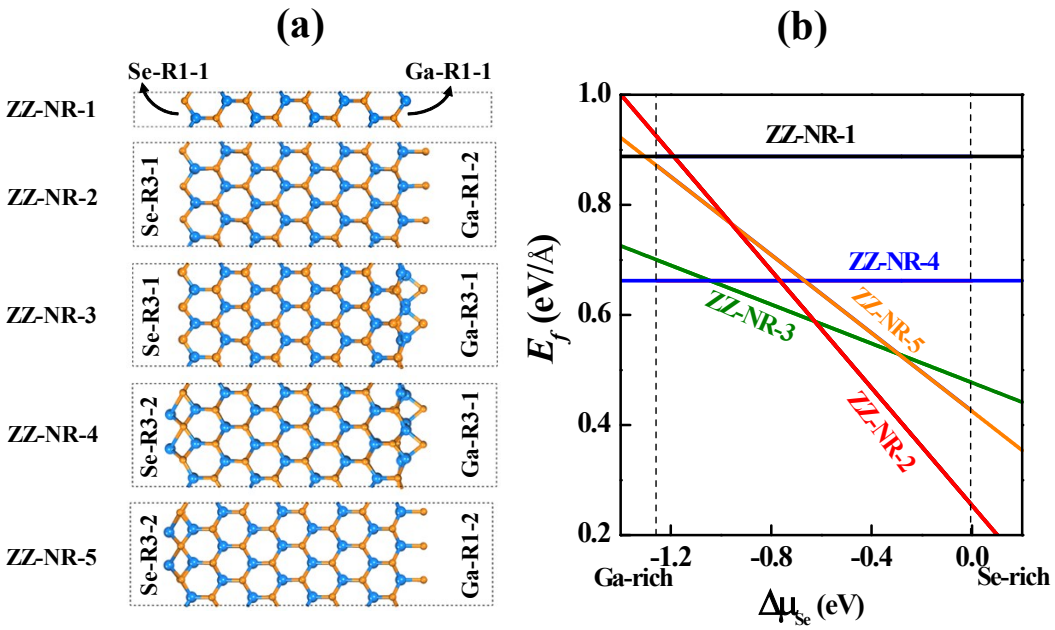

Fig. S6 (a) Atomic configurations of zigzag GaSe nanoribbons and (b) formation energies of the nanoribbons as a function of Se chemical potential difference ($\Delta\mu_{Se}$). Here ZZ-NR-1 is the zigzag nanoribbon (ZZ-NR) with the Ga-R1-1 and Se-R1-1 edges, ZZ-NR-2 is the ZZ-NR with the Ga-R1-2 and Se-R3-1 edges, ZZ-NR-3 is the ZZ-NR with the Ga-R3-1 and Se-R3-1 edges, ZZ-NR-4 is the ZZ-NR with the Ga-R3-1 and Se-R3-2 edges, and ZZ-NR-5 is the ZZ-NR with the Ga-R1-2 and Se-R3-2 edges.

S6. Spin-projected DOS of GaSe nanoribbons

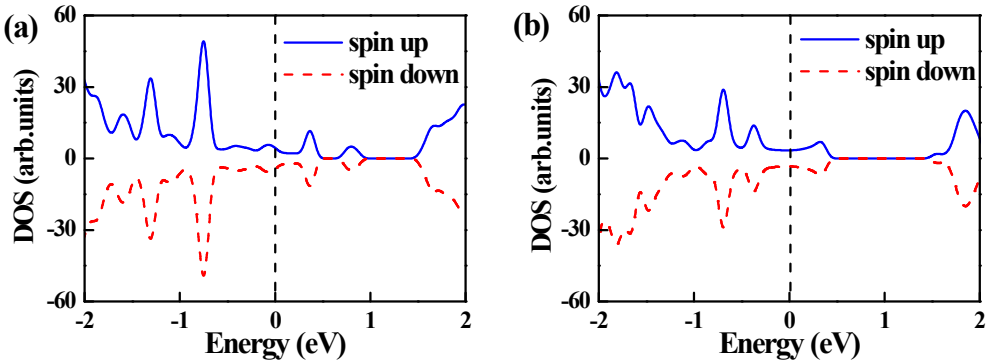

Fig. S7 The spin-projected density of states of (a) ZZ-NR-1 and (b) AC-NR-2. The solid and dash lines denote spin-up and spin-down DOS, respectively. The vertical dash lines denote the position of Fermi level.

S7. Charge-density distributions of VBM and CBM of GaSe nanoribbons

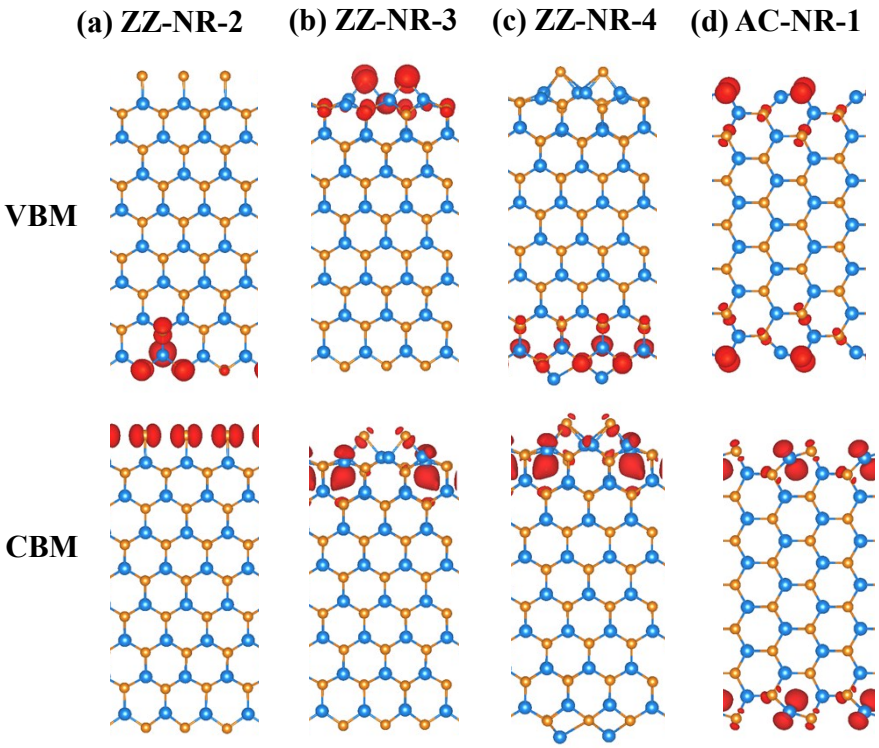

Fig. S8 Charge-density isosurface distributions of VBM and CBM states in four semiconducting GaSe nanoribbons, including (a) ZZ-NR-2, (b) ZZ-NR-3, (b) ZZ-NR-4, and (d) AC-NR-1.

S8. Band gaps of GaSe nanosheet and nanoribbons

Table S1 The band gaps (E_g) of GaSe nanosheet and nanoribbons calculated by using the PBE and HSE06 methods.

E_g (eV)	Nanosheet	ZZ-NR-2	ZZ-NR-3	ZZ-NR-4	AC-NR-1
PBE	2.22	0.05	1.14	0.89	1.29
HSE06	3.12	0.08	1.80	1.59	2.02

S9. Band structures of InSe nanoribbons

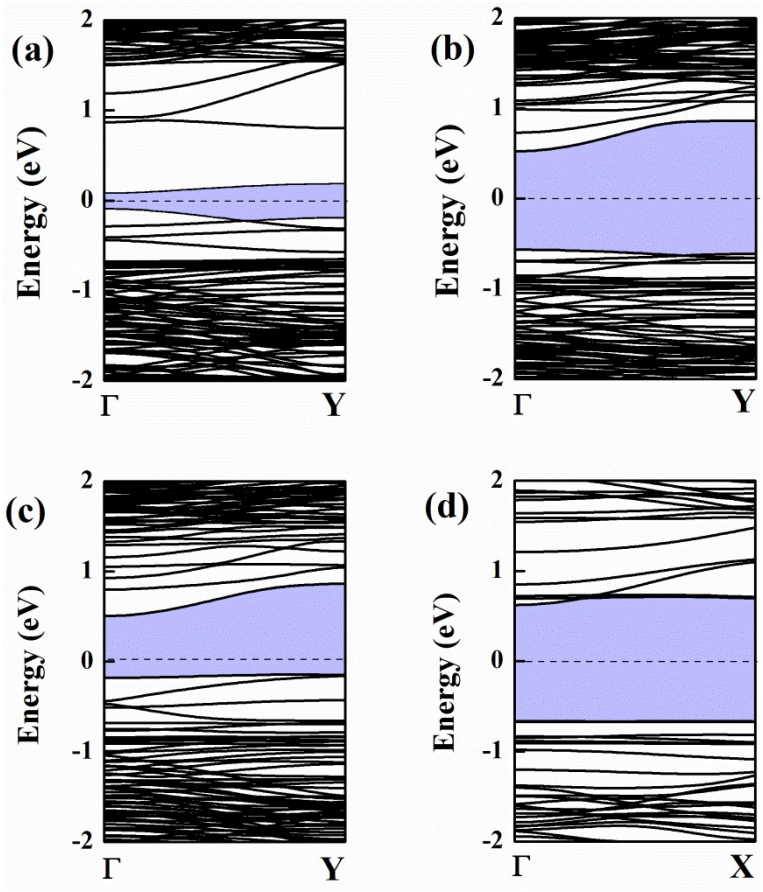

Fig. S9 Band structures of InSe nanoribbons. The band structure of (a) ZZ-NR with the In-R1-2 and Se-R3-1 edges (ZZ-NR-2), (b) ZZ-NR with the In-R3-1 and Se-R3-1 edges (ZZ-NR-3), (c) ZZ-NR with the In-R3-1 and Se-R3-2 edges (ZZ-NR-4), and (d) AC-NR with the AC-P edges (AC-NR-1). The dash lines denote the position of Fermi level.

S10. Band structures of GaSe nanoribbons from the HSE06 method

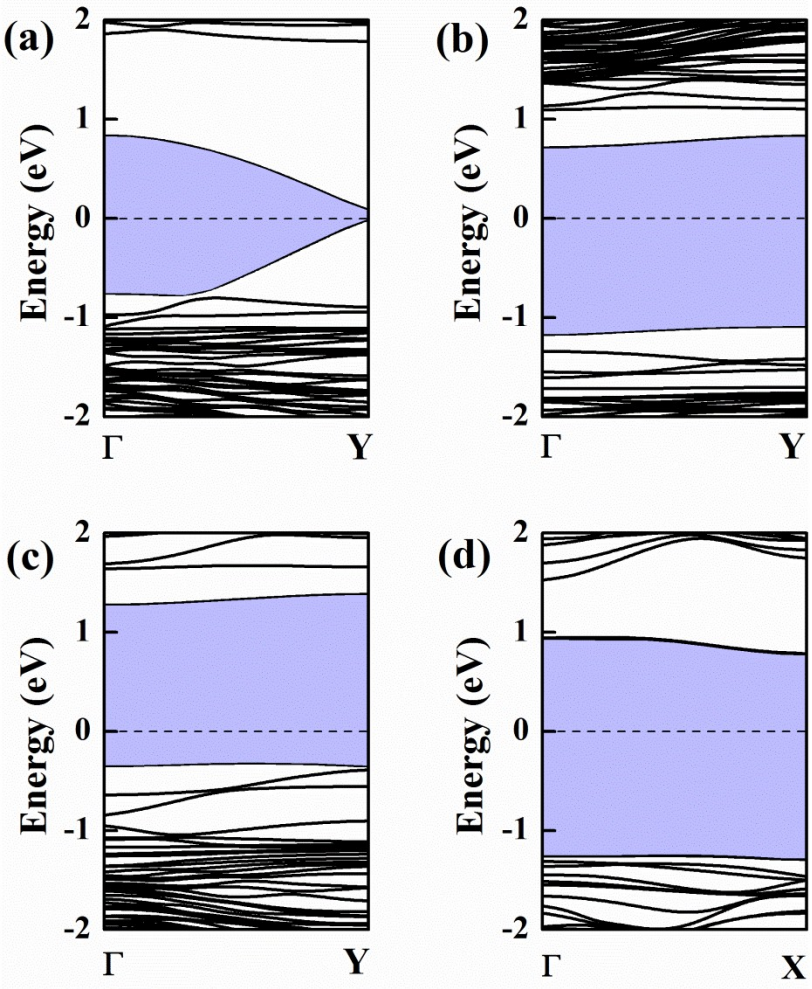

Fig. S10 Band structures of (a) ZZ-NR-2, (b) ZZ-NR-3, (c) ZZ-NR-4, and (d) AC-NR-1 from the HSE06 method. The horizontal dash lines denote the position of Fermi level.

S11. Size-dependent band gap of armchair GaSe nanoribbons

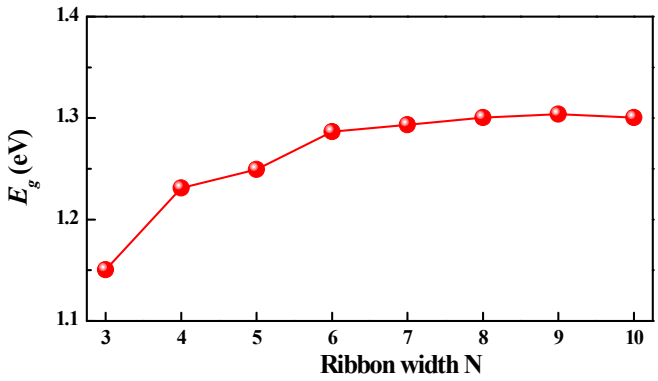

Fig. S11 The band gap (E_g) of armchair GaSe nanoribbon with the perfect edges (AC-P) as a function of ribbon width N.

S12. PDOS of zigzag and armchair GaSe nanoribbons

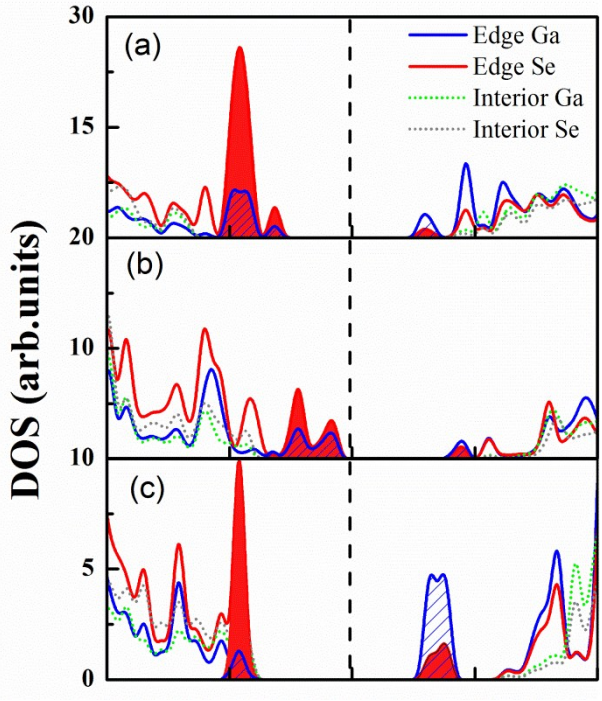

Fig. S12 The partial density of states of (a) ZZ-NR-3, (b) ZZ-NR-4, and (c) AC-NR-1. The ribbon width is set to N =6 for all three GaSe NRs. The filled and shadowed regions denote the electronic states of Ga and Se atoms at NR edges contributed to the band-edge states, respectively. The vertical dash lines denote the position of Fermi level.

S13. Movie for illustrating the shape evolution of GaSe flakes

Movie S1 shows an animation illustrating the shape evolution of GaSe flakes as the chemical potential $\Delta\mu_{Se}$ is varied.

References

1 Y. Liu, S. Bhowmick and B. I. Yakobson, *Nano Lett.* 2011, **11,** 3113-3116.

2 Y. Liu, A. Dobrinsky and B. I. Yakobson, *Phys. Rev. Lett.* 2010, **105**, 235502.

3 D. Cao, T. Shen, P. Liang, X. S. Chen and H. B. Shu, *J. Phys. Chem. C* 2015, **119**, 4294-4301.